CHEMISTRY OF MATERIALS
Article

Chem. Mater. **2009,** *21,* 4541–4554 4541
DOI:10.1021/cm901492f

Controlled Synthesis of Semiconducting Metal Sulfide Nanowires

Fen Zhang[†] and Stanislaus S. Wong*[,†,‡]

[†]*Department of Chemistry, State University of New York at Stony Brook, Stony Brook, New York 11794-3400, and* [‡]*Condensed Matter Physics and Materials Sciences Department, Brookhaven National Laboratory, Building 480, Upton, New York 11973*

Received May 31, 2009. Revised Manuscript Received July 27, 2009

We describe the preparation and characterization of (a) discrete, individual motifs and (b) arrays of crystalline and pure semiconducting transition metal sulfide (CuS, PbS, and CdS) nanowires, synthesized via an inexpensive, generalizable, simplistic, and ambient modified template-directed technique. We have demonstrated control over the diameters and lengths of our one-dimensional (1-D) nanostructures through corresponding variations in the template membrane's pore size and thickness. We have not only successfully generated cubic-phase 1-D CdS nanowires but also produced, at slightly elevated temperatures, unusual CdS cactus-like, hierarchical nanostructures, consisting of tiny nanoneedles projecting out from the outer surfaces of parent CdS nanotube motifs. Opto-vibrational properties of all of these metal sulfide nanomaterials have been extensively studied. In addition, our results indicate that our as-prepared hexagonal-phase CdS cactus-like nanotubes evinced a higher photocatalytic degradation activity than that of both cubic CdS nanowires and their commercial bulk counterparts.

Introduction

Nanomaterials, that is, structures with at least one dimension between 1 and 100 nm, includes a host of substances and are fundamentally interesting due to their fascinating size-dependent optical, electronic, magnetic, thermal, mechanical, chemical, and physical properties, which are distinctive not only from their bulk counterparts but also from the atomic or molecular precursors from whence they were derived.[1,2] In particular, semiconducting metal sulfide nanoparticulates possess novel optical and electrical properties and are considered as building blocks for photovoltaic devices including dye-sensitized cells, all-inorganic nanoparticle solar cells, and hybrid nanocrystal−polymer composite solar cells in addition to lasers and waveguides.

Specifically, green covellite copper sulfide (CuS)[3−7] possesses metal-like electrical conductivity and chemical sensing capabilities. CuS films maintain transmittance in the infrared, low reflectance in the visible, and relatively high reflectance in the near-infrared region, which are ideal characteristics for solar energy adsorption. Moreover, CuS transforms into a superconductor at 1.6 K[8,9] and has recently been used as a cathode material in lithium rechargeable batteries.[10]

Cadmium sulfide (CdS) is a II−VI semiconductor with a direct band gap of 2.42 eV with potential applications in laser light-emitting diodes, displays, dye-sensitized solar cells, fluorescence probes, sensors, photoelectrocatalysts, waveguides, and optoelectronic devices, based on its nonlinear optical properties.[11−19] Very recently, in a manner analogous to ZnO, upon visible light illumination, CdS nanowires have been used to convert mechanical energy into electricity by carefully coupling the piezoelectric, optoelectronic, and semiconducting properties of these materials.[20,21]

As a narrow band gap semiconductor with a bulk band gap energy of 0.41 eV, lead sulfide (PbS) has a reasonably large exciton Bohr radius of 18 nm, which allows it to achieve stronger confinement effects, even at relatively

*To whom correspondence should be addressed. Phone: 631-632-1703; 631-344-3178. E-mail: sswong@notes.cc.sunysb.edu; sswong@bnl.gov.

(1) Xia, Y.; Yang, P.; Sun, Y.; Wu, Y.; Mayers, B.; Gates, B.; Yin, Y.; Kim, F.; Yan, H. *Adv. Mater.* **2003**, *15*(5), 353–389.
(2) Mao, Y.; Park, T.-J.; Zhang, F.; Zhou, H.; Wong, S. S. *Small* **2007**, *3*(7), 1122–1139.
(3) Wang, X.; Xu, C.; Zhang, Z. *Mater. Lett.* **2006**, *60*(3), 345–348.
(4) Liang, W.; Whangbo, M. H. *Solid State Commun.* **1993**, *85*, 405–408.
(5) Mane, R. S.; Lokhande, C. D. *Mater. Chem. Phys.* **2000**, *65*, 1–31.
(6) Janata, J.; Josowicz, M.; DeVaney, D. M. *Anal. Chem.* **1994**, *66*, 207–228.
(7) Liao, X. H.; Chen, N. Y.; Xu, S.; Yang, S. B.; Zhu, J. J. *J. Cryst. Growth* **2003**, *252*, 593–598.
(8) Blachnik, R.; Müller, A. *Thermochim. Acta* **2000**, *361*, 31–52.
(9) Zhang, W.; Wen, X.; Yan, S. *Langmuir* **2003**, *19*, 4420–4426.
(10) Chung, J.-S.; Sohn, H.-J. *J. Power. Source* **2002**, *108*, 226–231.
(11) Henglein, A. *Chem. Rev.* **1989**, *89*, 1861–1873.
(12) Barrelet, C. J.; Wu, Y.; Bell, D. C.; Lieber, C. M. *J. Am. Chem. Soc.* **2003**, *125*, 11498–11499.
(13) Bao, N.; Shen, L.; Takata, T.; Domen, K.; Gupta, A.; Yanagisawa, K.; Grimes, C. A. *J. Phys. Chem. C* **2007**, *111*, 17527–17534.
(14) Britt, J.; Ferekides, C. *Appl. Phys. Lett.* **1993**, *62*, 2851–2852.
(15) Brus, L. E.; Efros, A. L.; Itoh, T. *J. Lumin.* **1996**, *76*, 1.
(16) Morales, A. M.; Lieber, C. M. *Science* **1998**, *279*, 208–211.
(17) Wang, Z. L. *Adv. Mater.* **2000**, *12*, 1295–1298.
(18) Tsai, C. T.; Chuu, D. S.; Chen, G. L.; Yang, S. L. *J. Appl. Phys.* **1996**, *79*, 9105–9109.
(19) Berman, A.; Charych, D. *Adv. Mater.* **1999**, *11*, 296–300.
(20) Lin, Y.-F.; Song, J.; Ding, Y.; Lu, S.-Y.; Wang, Z. L. *Appl. Phys. Lett.* **2008**, *92*, 022105/1–022105/3.
(21) Lin, Y.-F.; Song, J.; Ding, Y.; Lu, S.-Y.; Wang, Z. L. *Adv. Mater.* **2008**, *20*, 3127–3130.

Published on Web 09/16/2009

larger dimensions.[22,23] Hence, PbS is an extremely promising material for a large number of applications in mid- and near-infrared emission and detection,[23−25] important for biology and sensing.[26] Moreover, it has found usage in optoelectronic devices,[27,28] including light emitting diodes, flame monitors, photovoltaics, solar cells, and high-speed optical switches, due to its third order nonlinear optical properties.[22,29−32]

In recent years, high-quality semiconducting one-dimensional (1D) nanostructures, such as nanowires and nanotubes, with their inherent anisotropy, have been considered as model systems for the efficient transport of electrons and optical excitations. As such, semiconducting nanowires have been used as building blocks for a number of nanoscale energy-conversion, photonic, and electro-optical devices (including field-effect transistors, light-emitting diodes, logic gates, lasers, waveguides, and solar cells), as well as electronic circuits.[33,34] Nevertheless, a lot of significant effort, summarized in the Supporting Information section, has been expended in overcoming numerous challenges associated with the goal of achieving a controlled synthesis of semiconducting nanowires with reproducible morphology, crystallinity, chemical composition, and monodispersity.

It is obvious based on all of the prior work that it would be desirable to develop a protocol that allows for a green, cost-effective methodology of metal sulfide 1D nanoscale synthesis without the need to sacrifice on sample quality, crystallinity, monodispersity, and purity. That is, it would be a viable, complementary advance to develop a generalizable protocol aimed at CuS, CdS, and PbS nanowire/array formation. Such a methodology would overcome (i) the high-temperatures, (ii) the need for expensive, complicated equipment, (iii) the use of potentially toxic, gaseous precursors and byproducts, (iv) the utilization of costly catalysts and performance-altering capping agents (including surfactants), or (v) the polycrystallinity of the ultimate product, characteristic of a number of previous literature methods of sulfide nanoscale metal synthesis.

As a straightforward route, therefore, template synthesis enables a high degree of control over the dimensions (i.e., mean diameters and diameter distributions) of the resulting 1D nanostructures. Prior literature has suggested that the fabrication of PbS, CuS, and CdS nanorods can occur either by electrodeposition or injection of reactants within the channel pores of either anodic aluminum oxide[35−41] or mesoporous silica[42−44] templates. As drawbacks in terms of sample quality and reaction conditions, though, nanostructures synthesized using this traditional template method often either are polycrystalline or necessitate an additional annealing step at high temperature. Our group has recently expended significant effort in devising a simple and versatile variation of the template technique that can operate well under ambient conditions in aqueous solution.

We have successfully demonstrated the validity of this protocol through the production of 1D nanostructures of a number of classes of diverse materials, including oxides (ZnO, CuO, α-Fe_2O_3, $BaCrO_4$, $BaWO_4$, $CaWO_4$, $SrWO_4$, associated solid-solution analogues $Sr_{1-x}Ca_xWO_4$ and $Ba_{1-x}Sr_xWO_4$ ($0 < x < 1$), doped tungstates, and $MnWO_4$) and fluorides (BaF_2, CaF_2, SrF_2, NH_4MnF_3, and $KMnF_3$).[45−52] The gist of the method is that we initially mount conventional, commercially available membranes, composed of either alumina or polymer, between the two halves of a U-tube cell.[53,54] The half-cells are then filled with solutions of precursors at concentrations targeted so as to yield desired molar stoichiometries of relevant elements in the final products. In effect, the pores in the membranes are used as the localized environment within which to spatially confine and control the growth of our one-dimensional products. Moreover, these as-produced nanomaterials are chemically pure, are structurally well-defined, and can be generated in reasonable quantities. The key point is that our method is generalizable and can be adapted to the

(22) Peterson, J. J.; Krauss, T. D. *Nano Lett.* **2006**, *6*, 510–514.
(23) Gadenne, P.; Yagil, Y.; Deutscher, G. *J. Appl. Phys.* **1989**, *66*, 3019–3025.
(24) McDonald, S. A.; Konstantatos, G.; Zhang, S.; Cyr, P. W.; Klem, E. J. D.; Levina, L.; Sargent, E. H. *Nat. Mater.* **2005**, *4*, 138–142.
(25) Bakueva, L.; Konstantatos, G.; Levina, L.; Musikhin, S.; Sargent, E. H. *Appl. Phys. Lett.* **2004**, *84*, 3459–3461.
(26) Bakueva, L.; Gorelikov, I.; Muskhin, S.; Zhao, X. S.; Sargent, E. H.; Kumacheva, E. *Adv. Mater.* **2004**, *16*, 926–929.
(27) Lu, W.; Fang, J.; Ding, Y.; Wang, Z. L. *J. Phys. Chem. B* **2005**, *109*, 19219–19222.
(28) Schaller, R. D.; Petruaka, M. A.; Klimov, V. I. *J. Phys. Chem. B* **2003**, *107*, 13765–13768.
(29) Wang, Z. L.; Zhao, B.; Zhang, F.; Mao, W.; Qian, G.; Fan, X. *Mater. Lett.* **2007**, *61*, 3733–3735.
(30) Hirata, H.; Higashiayama, K. *Bull. Chem. Soc. Jpn.* **1971**, *44*, 2420–2423.
(31) Plass, R.; Pelet, S.; Krueger, J.; Gratzel, M.; Bach, U. *J. Phys. Chem. B* **2002**, *106*, 7578–7580.
(32) Warner, J. H.; Watt, A. A. R.; Tilley, D. R. *Nanotechnology* **2005**, *16*, 2381–2384.
(33) Sun, J.; Buhro, W. E. *Angew. Chem., Int. Ed.* **2008**, *47*, 3215–3218.
(34) Wang, J.; Gudiksen, M. S.; Duan, X.; Cui, Y.; Lieber, C. M. *Science* **2001**, *293*, 1455.
(35) Chen, J.-H.; Chao, C.-G.; Ou, J.-C.; Liu, T.-F. *Surf. Sci.* **2007**, *601*, 5142–5147.
(36) Singh, K. V.; Martinez-Morales, A. A.; Bozhilov, K. N.; Ozkan, M. *Chem. Mater.* **2007**, *19*, 2446–2454.
(37) Routkevitch, D.; Haslett, T. L.; Ryan, L.; Bigioni, T.; Douketis, C.; Moskovits, M. *Chem. Phys.* **1996**, *210*, 343–352.
(38) Suh, J. S.; Lee, J. S. *Chem. Phys. Lett.* **1997**, *281*, 384–388.
(39) Li, Y.; Xu, D.; Zhang, Q.; Chen, D.; Huang, F.; Xu, Y.; Guo, G.; Gu, Z. *Chem. Mater.* **1999**, *11*, 3433–3435.
(40) Xu, D.; Chen, D.; Xu, Y.; Shi, X.; Guo, G.; Gui, L.; Tang, Y. *Pure Appl. Chem.* **2000**, *72*, 127–135.
(41) Xu, D.; Xu, Y.; Chen, D.; Guo, G.; Gui, L.; Tang, Y. *Adv. Mater.* **2000**, *12*, 520–522.
(42) Thiruvengadathan, R.; Regev, O. *Chem. Mater.* **2005**, *17*, 3281–3287.
(43) Gao, F.; Lu, Q.; Zhao, D. *Adv. Mater.* **2003**, *15*, 739–742.
(44) Gao, F.; Lui, Q.; Liu, X.; Yan, Y.; Zhao, D. *Nano Lett.* **2001**, *1*, 743–748.
(45) Mao, Y.; Wong, S. S. *J. Am. Chem. Soc.* **2004**, *126*, 15245–15252.
(46) Mao, Y.; Wong, S. S. *J. Am. Chem. Soc.* **2006**, *128*, 8217–8226.
(47) Mao, Y.; Zhang, F.; Wong, S. S. *Adv. Mater.* **2006**, *18*, 1895–1899.
(48) Zhou, H.; Wong, S. S. *ACS Nano* **2008**, *2*(5), 944–958.
(49) Zhou, H.; Yiu, Y.; Aronson, M. C.; Wong, S. S. *J. Solid State Chem.* **2008**, *181*(7), 1539–1545.
(50) Zhang, F.; Mao, Y.; Park, T.-J.; Wong, S. S. *Adv. Funct. Mater.* **2008**, *18*(1), 103–112.
(51) Zhang, F.; Sfeir, M. Y.; Misewich, J. A.; Wong, S. S. *Chem. Mater.* **2008**, *20*(17), 5500–5512.
(52) Zhang, F.; Yiu, Y.; Aronson, M. C.; Wong, S. S. *J. Phys. Chem. C* **2008**, *112*(38), 14816–14824.
(53) Martin, C. R.; Van Dyke, S. V.; Cai, Z.; Liang, W. *J. Am. Chem. Soc.* **1990**, *112*, 8976–8977.
(54) Liang, W.; Martin, C. R. *Chem. Mater.* **1991**, *3*, 390–391.

production of families of metal sulfides, which are the focus of our efforts herein.

Experimental Section

Synthesis. Polycarbonate track-etch membranes of approximately 6 μm in thickness, containing pore sizes of 50, 100, and 200 nm diameter, respectively, were purchased from Whatman Co., U.K. The membranes were initially hydrated by immersion and sonication in a small volume of distilled, deionized water for a few minutes, so as to limit the formation of air bubbles either within their interior pore channels or on the membrane surfaces. To avoid unwanted particle formation and deposition onto the external surfaces of the polycarbonate (PC) membranes, microcontact printed OTS-SAMs (octadecyltetrachlorosilane self-assembled monolayers) were used as passivation layers.[55] Hence, a homemade PDMS (polydimethylsiloxane) stamp was initially inked with a 10 mM hexane solution of OTS and dried with nitrogen. The stamp was then placed into contact with the PC membranes for 30 s and then peeled off carefully.

Subsequently, the membrane was mounted between two half arms of a U-shaped tube. Precursors Na_2S (Alfa Aesar, 98%), $Cu(NO_3)_3$ (Alfa Aesar, 98%), $Pb(CH_3COO)_2$ (Aldrich, 99.99%), and $Cd(NO_3)_2$ (Alfa Aesar, 98.5%) were of analytical grade and were used without further purification. In a typical synthesis, one of the two half-cells was filled with freshly prepared 0.01 M Na_2S solution, which was adjusted to pH = 6 using HCl. The other half-cell contained a 0.01 M solution of $Cu(NO_3)_2$, $Pb(CH_3COO)_2$, or $Cd(NO_3)_2$, used to generate CuS, PbS, or CdS nanowires, respectively. The system was then left unperturbed for an incubation period of as little as 5 h and up to 12 h at temperatures ranging from ambient conditions to 80 °C. In the specific cases of CuS and PbS, such temporal and thermal variations did not appreciably affect either the morphology or the composition of the resultant products (Figure S1, Supporting Information). By contrast, as we will discuss, an increase in reaction temperature to 80 °C resulted in the transformation of cubic zinc blende CdS nanowires into hexagonal würtzite cactus-like CdS nanostructures.

Subsequent to precursor solution immersion and product formation, either a black color (CuS and PbS) or a yellow hue (CdS) was observed, associated with the polycarbonate membrane, which was then detached, sonicated for ~2 min to remove unwanted particles on the surface, and thoroughly washed with distilled water, prior to dissolution and removal with methylene chloride. As-prepared sulfide nanowires were then collected and isolated from solution by centrifugation after washing.

Characterization. As-prepared samples were thoroughly characterized using a number of different methodologies, including powder X-ray diffraction (XRD), field-emission scanning electron microscopy (FE-SEM), transmission electron microscopy (TEM), high resolution TEM (HRTEM), selected area electron diffraction (SAED), and energy-dispersive X-ray spectroscopy (EDX), as well as with Raman, UV−visible, and photoluminescence (PL) spectroscopies.

X-ray Diffraction. Crystallographic and purity information on as-prepared sulfide nanowires were initially obtained using powder X-ray diffraction (XRD). To prepare analyzable samples, the resulting sulfide nanowires were rendered into slurries in ethanol, sonicated for ~1 min, and then air-dried upon deposition onto glass slides. Diffraction patterns were collected using a Scintag diffractometer, operating in the Bragg configuration using Cu Kα radiation (λ = 1.54 Å) from 10 to 80° at a scanning rate of 2°/min.

Electron Microscopy. The morphology and size of the resulting sulfide nanowires were initially characterized using a field emission SEM (FE-SEM Leo 1550) at accelerating voltages of 15 kV, which was equipped with EDS capabilities. Specifically, samples for SEM were prepared by dispersing as-prepared sulfide nanowires in ethanol, sonicating for ~2 min, and then depositing these nanostructures onto a silicon wafer, attached to a SEM brass stub using conductive carbon tape. All of these samples were subsequently conductively coated with gold by sputtering for 15 s, so as to minimize charging effects under SEM imaging conditions.

Low-magnification TEM images were taken at an accelerating voltage of 80 kV on a FEI Tecnai12 BioTwinG^2 instrument, equipped with an AMT XR-60 CCD Digital Camera System. High-resolution TEM (HRTEM) images and SAED patterns were obtained on a JEOL 2010F instrument at accelerating voltages of 200 kV. Specimens for all of these TEM experiments were prepared by sonicating the as-prepared product for 2 min in ethanol to ensure adequate dispersion of the nanowires and placing one drop of the solution onto a 300 mesh Cu grid, coated with a lacey carbon film.

Optical Spectroscopy. Raman spectra were obtained on solid samples dispersed in ethanol and placed onto a Si wafer. Spectra were obtained on a Renishaw 1000 Raman microspectrometer with excitation from argon ion (514.5 nm), He−Ne (632.8 nm), and diode (780 nm) lasers, respectively, at a power level of 5 mW. In addition, a Renishaw System 1000 microscope with a tunable argon ion laser was used to acquire Raman data at 488 nm excitation. A 50× objective and low laser power density were used for the irradiation of the sample and for signal collection. The laser power was kept sufficiently low to avoid heating of the samples by optical filtering and/or defocusing of the laser beam at the sample surface. Spectra were collected in the range of 3000−100 cm^{-1} with a resolution of 1 cm^{-1}.

UV−visible spectra were collected at high resolution with a Thermospectronics UV1 spectrometer using quartz cells with a 10-mm path length. Spectra were obtained for as-prepared sulfide nanorods, which were previously sonicated in distilled water so as to yield homogeneous dispersions. UV−visible absorption spectra were recorded using distilled water as a blank.

Samples for PL spectra were dispersed in deionized water and sonicated for 1 min. Fluorescence data were obtained at room temperature on a Jobin Yvon Spex FluoroMax-4 instrument with a 10 s integration time. PL spectra for CuS, PbS, and CdS nanostructures were measured at excitation wavelengths of 370, 495, and 400 nm, respectively, in accordance with the literature.

Photocatalytic Degradation Activity. In a typical experiment, the CdS powdered catalyst (with a resulting concentration of 0.5 g/L), suspended in an aqueous solution of either 50 ppm Rhodamine B or methyl orange, was ultrasonicated for 10 min and magnetically stirred under dark, unilluminated conditions for 30 min so as to establish an adsorption−desorption equilibrium with respect to the individual dye species. After given irradiation time intervals with UV light at 366 nm at a 5 cm separation distance, the photocatalytic performance of the various CdS nanoscale catalysts was subsequently gauged by measuring changes in the intensity of the optical absorbance peaks, localized at either 555 or 464 nm, of the aqueous supernatant aliquots containing either Rhodamine B or methyl orange dye species, respectively. Analogous control experiments

(55) Kumar, A.; Whitesides, G. M. *Appl. Phys. Lett.* **1993**, *63*, 2002–2004.

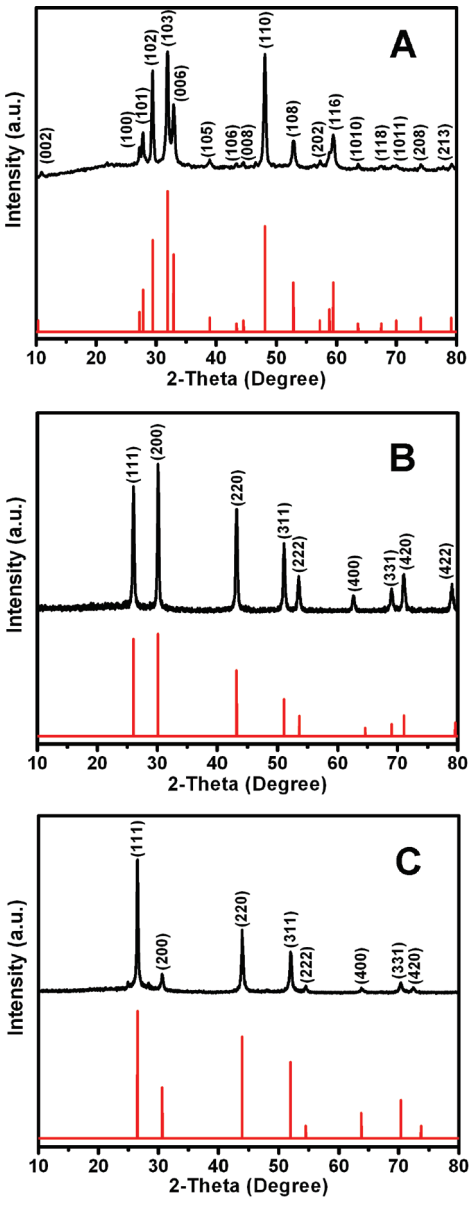

Figure 1. XRD patterns obtained from (A) as-prepared CuS nanowires (top, black) and corresponding JCPDS No. 06-0464 database standard for CuS (bottom, red); (B) as-prepared PbS nanowires (top, black) and corresponding JCPDS No. 78-1901 database standard for PbS (bottom, red); (C) as-prepared CdS nanowires (top, black) and corresponding JCPDS No. 10-0454 database standard for CdS (bottom, red).

were performed either without CdS (blank) or in the presence of a commercial bulk sample (CERAC Inc.; particle size corresponding to −325 mesh or $< 64\ \mu$m), normalized for identical metal sulfide concentrations.

Results and Discussion

X-ray Diffraction. The purity and crystallinity of as-prepared sulfide nanowire samples were initially characterized using powder X-ray diffraction (XRD) measurements (Figure 1, A−C). As shown in Figure 1 and summarized in Table S1, all of the diffraction peaks observed from each of the samples can be readily indexed and have been positively ascribed to pure phases of their bulk counterparts, with lattice constants comparable to the corresponding reported database values, associated with each of the target materials. Very little if any impurity peaks were present in any of the patterns, though it should be mentioned that two very weak peaks surrounding the (111) peak of cubic phase CdS (JCPDS No. 10-0454) in Figure 1C could be ascribed to the (100) and (101) peaks of hexagonal würtzite CdS (JCPDS No. 41-1049). Thus, overall, these results strongly suggest that reasonably pure, crystalline hexagonal-phase CuS, cubic-phase PbS, and cubic-phase CdS can be prepared under ambient, room-temperature conditions without the necessity of an additional annealing step at high temperature.

The CdS results are worthy of further discussion. CdS possesses three types of crystal structures, namely, hexagonal würtzite, cubic zinc blende, and high-pressure rocksalt phases. The hexagonal phase can be observed in both bulk and nanocrystalline structures, whereas the cubic and rocksalt phases are less commonly formed.[42] Among the three phases, hexagonal würtzite has been intensively investigated because it is the most thermodynamically stable form of CdS and has been extensively synthesized easily by a number of groups.[43,56−59] By contrast, only a relatively few number of papers has ever claimed the synthesis of either spherical quantum dots or cylindrical nanowires of CdS possessing either the cubic zinc blende phase or even a mixture of both hexagonal and cubic phases.[13,42,60,61] Hence, our work is significant in that, to the best of our knowledge, for the first time, we have demonstrated the ambient, room-temperature preparation of CdS nanowires associated with a metastable cubic phase with minimal hexagonal phase impurities.

Figure S2 (Supporting Information) shows the XRD patterns of CdS nanostructures prepared at 80 °C. In contrast with ambiently prepared cubic phase CdS nanowires, all of the diffraction peaks corresponding to the cactus-like nanostructures, formed at higher temperatures, can be indexed to the pure hexagonal phase of CdS (JCPDS No. 41-1049). We note that the energy difference between the cubic and hexagonal CdS energy gap differs by less than 0.1 eV.[62] Hence, our observations are not surprising since it has been reported that, at low temperatures, the cubic phase can be more easily obtained whereas at higher temperatures, the hexagonal phase is more prevalent.[63−65] Moreover, the relative peak broadening observed can be attributed to the existence of

(56) Xiong, S.; Xi, B.; Wang, C.; Zou, G.; Fei, L.; Wang, W.; Qian, Y. *Chem.—Eur. J.* **2007**, *13*, 3076–3081.
(57) Xi, L.; Tan, W. X. W.; Boothroyd, C.; Lam, Y. M. *Chem. Mater.* **2008**, *20*, 5444–5452.
(58) Zhang, J.; Jiang, F.; Zhang, L. *J. Phys. Chem. B* **2004**, *108*, 7002–7005.
(59) Zhan, J. H.; Yang, X. G.; Wang, D. W.; Li, S. D.; Xie, Y.; Xia, Y.; Qian, Y. T. *Adv. Mater.* **2000**, *12*, 1348–1351.
(60) Simmons, B. A.; Li, S.; John, V. T.; McPherson, G. L.; Bose, A.; Zhou, W.; He, J. *Nano Lett.* **2002**, *2*, 263–268.
(61) Sathish, M.; Viswanath, R. P. *Catal. Today* **2007**, *129*, 421–427.
(62) Zelaya-Angel, O.; Alvarado-Gil, J.; Lozada-Morales, R.; Vargas, H.; Ferreira da Silva, A. *Appl. Phys. Lett.* **1994**, *64*(3), 291–293.
(63) Chen, Q.; Bao, H.; Shen, X. *Phase Transitions* **2008**, *81*(6), 591–601.
(64) Narayanan, K. L.; Vijayakumar, K. P.; Nair, K. G. M.; Thampi, N. S.; Krishan, K. *J. Mater. Sci.* **1997**, *32*, 4837–4840.
(65) Bandaranayake, R. J.; Wen, G. W.; Lin, J. Y.; Jiang, H. X.; Sorensen, C. M. *Appl. Phys. Lett.* **1995**, *67*(6), 831–833.

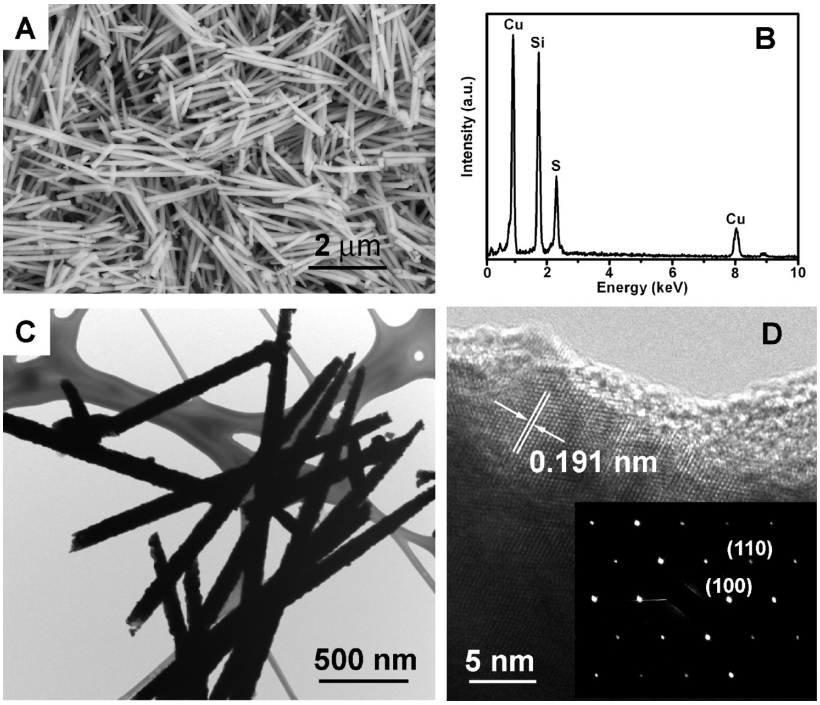

Figure 2. (A, C) Typical SEM and TEM images of as-prepared CuS nanowires, prepared using polycarbonate membranes with 100-nm pore diameters. (B) EDS spectrum of as-prepared CuS nanowires. The Si peak originates from the underlying silicon wafer. (D) HRTEM image of a representative portion of an individual CuS nanowire shown in (C). Corresponding SAED patterns are shown in the inset.

crystalline faults, microstrains, crystalline domain sizes, and/or domain size distribution.[66]

Electron Microscopy. (*i*) *CuS*. The size and morphology of as-prepared metal sulfide 1D nanostructures have been studied using FE-SEM and TEM. Figure 2, panels A and C, show typical SEM and TEM images of CuS nanowires, respectively, which had been fabricated using polycarbonate membranes with 100-nm diameter pore sizes. The presence of dispersed individual nanorods as well as of bundled, aggregated species clearly shows that straight, smooth, and crystalline wire-like CuS 1D nanostructures, with a relatively uniform diameter throughout their entire length, can be produced. Diameters of as-prepared CuS nanowires were 100 ± 13 nm, while measured lengths attained values of as much as several micrometers, comparable to the thickness (6 μm) of the PC membranes from whence these structures were derived. In addition, EDS elemental analysis data (Figure 2B) taken from SEM clearly indicate that the sample is only composed of Cu and S, as expected, with the presence of the Si peak attributable to the underlying silicon wafer.

To provide additional insight into the structure of the as-prepared sample, randomly chosen single nanowires, shown in Figure 2C, were analyzed by HRTEM and SAED. Figure 2D highlights the HRTEM image of a portion of an individual CuS nanowire, which is single-crystalline with a lattice fringe spacing of 0.191 nm, corresponding to the (110) plane of the hexagonal phase of a CuS crystal. The inset to Figure 2D shows the SAED pattern, consisting of sharp spots that can be indexed to the (110) and (100) diffraction planes, respectively, of primitive hexagonal CuS. These findings are consistent with observations from the XRD data shown in Figure 1A. Moreover, the HRTEM image and SAED patterns taken from different positions along the nanowire were found to be essentially identical within experimental accuracy, indicating the entire nanowire can be assumed to be single-crystalline, while a thin amorphous layer, visible in Figure 2D, likely coats at least part of the outer surface.

As a result of a high rate of occupancy of the interior of the membrane pores with the precursors associated with the CuS sample, the resulting nanowires tend to form arrays, after removal of the PC template by methylene chloride with modest sonication. As illustrated in Figure 3A, arrays of CuS nanowires appear to be structurally robust and well preserved. The SEM image in Figure 3B under higher magnification clearly shows that the nanowires are individually separated from each other as opposed to forming mass aggregates and are roughly parallel to each other so as to generate a packed, vertically aligned array architecture upon template removal.

It is evident that these nanowires form a dense, continuous network, stretching over micrometer-sized areas. In particular, Figure 3C,D presents the tilt and top views of CuS nanowire arrays, respectively, grown within the pores of PC templates. The diameters of these nanowires are $\sim 200 \pm 18$ nm, and their lengths measure in the micrometers, corresponding to the dimensions of the originating pore channels. We have not discounted the possibility that a remnant residue of the polycarbonate template, interdispersed within the nanowire framework,

(66) Shen, L.; Bao, N.; Yanagisawa, K.; Zheng, Y.; Domen, K.; Gupta, A.; Grimes, C. A. *J. Phys. Chem. C* **2007**, *111*, 7280–7287.

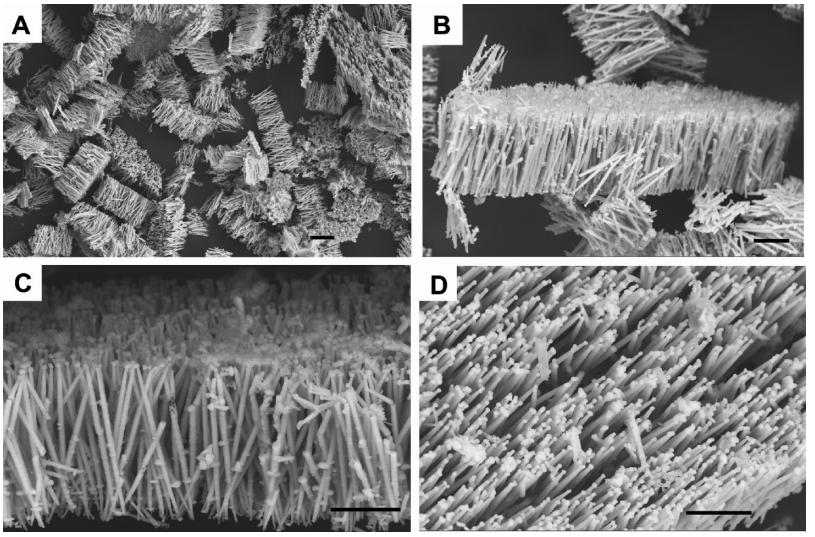

Figure 3. (A, B) Different magnification SEM images of CuS nanowire arrays, isolated from polycarbonate membranes containing 200-nm pore diameters. (C, D) Corresponding tilt-view and top-view SEM images of CuS nanowire arrays. Scale bars measure 2 μm.

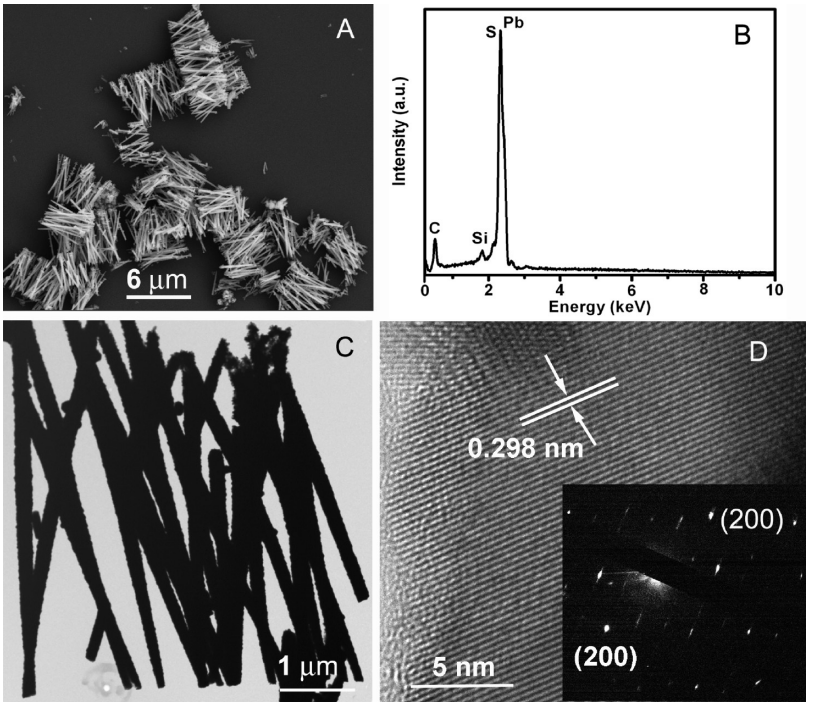

Figure 4. (A, C) Typical SEM and TEM images of as-prepared PbS nanowires, prepared using polycarbonate membranes containing 200-nm pore diameters. (B) EDS spectrum of as-prepared PbS nanowires. The C and Si peaks originate from the conductive carbon tape and silicon wafer, respectively. (D) HRTEM image of a representative portion of an individual PbS nanowire shown in (C). The corresponding SAED pattern is shown in the inset and is discussed in the text.

could be contributing to the mechanical support for these sulfide arrays. Such a scenario is not unusual considering that due to the random nature of the pore-production process in the track-etched membrane, a number of pores may have actually intersected within the membrane itself.[67] Moreover, while disulfide bond formation between dangling sulfur species is a plausible causal factor,[68] it is more likely that CuS growth "spilling" outside the pores themselves was a more important determinant, accounting for the additional reinforcing "glue" for these arrays.

(*ii*) *PbS*. Similarly, representative SEM and TEM images, as highlighted in panels A and C of Figure 4, respectively, reveal that clusters of as-prepared PbS, isolated from PC membranes with 200 nm pore size diameters, primarily consist of one-dimensional structures possessing a straight, wire-like morphology with a relatively uniform diameter in the range of 200 ± 20 nm throughout their entire length of approximately 3.7–5.6 μm. The EDS spectrum (Figure 4B) shows signals

(67) Hulteen, J. C.; Martin, C. R. *J. Mater. Chem.* **1997**, *7*(7), 1075–1087.
(68) Young, A. G.; Green, D. P.; McQuillan, A. J. *Langmuir* **2007**, *23*, 12923–12931.

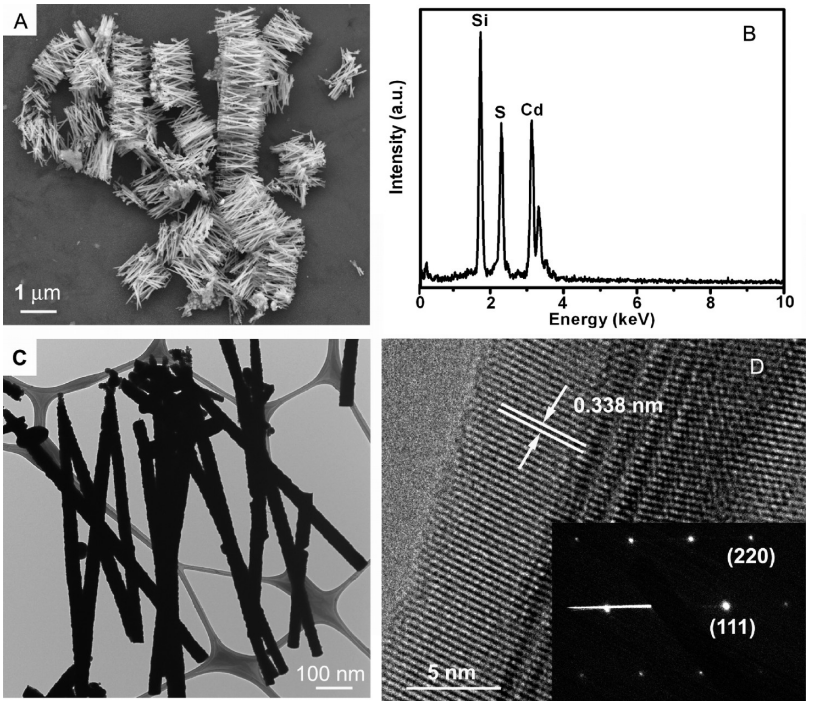

Figure 5. (A, C) Typical SEM and TEM images of as-prepared CdS nanowires, prepared using polycarbonate membranes with 50 nm pore diameters. (B) EDS spectrum of as-prepared CdS nanowires. The Si peak originates from the silicon wafer. (D) HRTEM image of a representative portion of an individual CdS nanowire shown in (C). The corresponding SAED pattern is shown in the inset.

associated with Pb and S, which overlap with each other in the energy scale at around 2.3−2.7 keV. The observed Si and C peaks likely originate from the silicon wafer and conductive carbon tape, respectively. The corresponding HRTEM image of a single PbS nanowire, shown in Figure 4D, suggests a lattice spacing of 0.298 nm, which can be indexed to the (200) plane of a face-centered cubic phase of a bulk PbS crystal (JCPDS File No. 78-1901), indicating that the nanowire likely grows in a [100] orientation. The somewhat distorted SAED pattern (inset to Figure 4D) suggests that the nanowires are not perfectly single-crystalline in nature. Indeed, the discrete but elongated bright spots can be indexed to the (200) planes of cubic PbS, unlike the usual broad, amorphous diffraction rings, characteristic of polycrystallinity. Moreover, the data indicate that the nanowire may consist of multiple single-crystalline domains composed of highly oriented nanocrystals growing along the [100] crystallographic axis.[69]

(*iii*) *CdS*. Panels A and C of Figure 5 present typical SEM and TEM images of an as-prepared CdS sample, respectively, prepared under ambient conditions. It can be observed that straight and smooth nanowires with relatively uniform and homogeneous size can be routinely synthesized. Measured nanowires possess diameters spanning from 46 to 53 nm, based on the corresponding 50 nm pore sizes of the PC membranes used, and a length range of 2.1 to 4.6 μm. The resulting nanowires also tend to form reasonably robust arrays upon removal of the template. The chemical signatures obtained from the EDS spectra (Figure 5B) correspond to Cd and S elements, as expected. The Si signal arises from the underlying silicon wafer used for analysis. A representative HRTEM image, shown in Figure 5D, illustrates the single-crystalline nature of the CdS nanowires with an interplanar spacing of ~0.338 nm, corresponding to the (111) plane of pure face-centered cubic CdS, which agrees with the XRD results initially shown in Figure 1C. The sharp SAED pattern in the inset confirms that the entire nanowire is likely single-crystalline in nature, with two diffraction planes, that is, (111) and (220), that can be indexed to the cubic structure of CdS.

As we have previously noted, nanoscale CdS structures, prepared at 80 °C, evinced a different morphological motif and crystallographic structure. Specifically, SEM (Figure 6A) and TEM (Figure 6C) images were suggestive of the formation of visibly roughened CdS nanotubes, possessing an inner diameter of ~78−90 nm, a wall thickness of ~4 nm, and average lengths of up to several micrometers. As indicated in the higher magnification image (inset to Figure 6C), the roughness of these nanotubes could be attributed to the formation of needle-like, ultrathin structures measuring ~20 nm long, projecting out, like a multitude of tiny bristles, from the surface of the outer wall. Though it is not an uncommon structural archetype, this cactus-like nanostructure has never, to the best of our knowledge, been previously observed for CdS. As the Si signal could be ascribed to the underlying silicon wafer used for SEM imaging, EDS analysis (Figure 6B) showed that the hollow structures were essentially composed of Cd and S, without any extraneous chemical impurity. Figure 6D illustrates a representative SAED pattern taken from an individual cactus-like nanostructure

(69) Tong, H.; Zhu, Y.-J.; Yang, L.-X.; Li, L.; Zhang, L. *Angew. Chem., Int. Ed.* **2006**, *45*, 7739–7742.

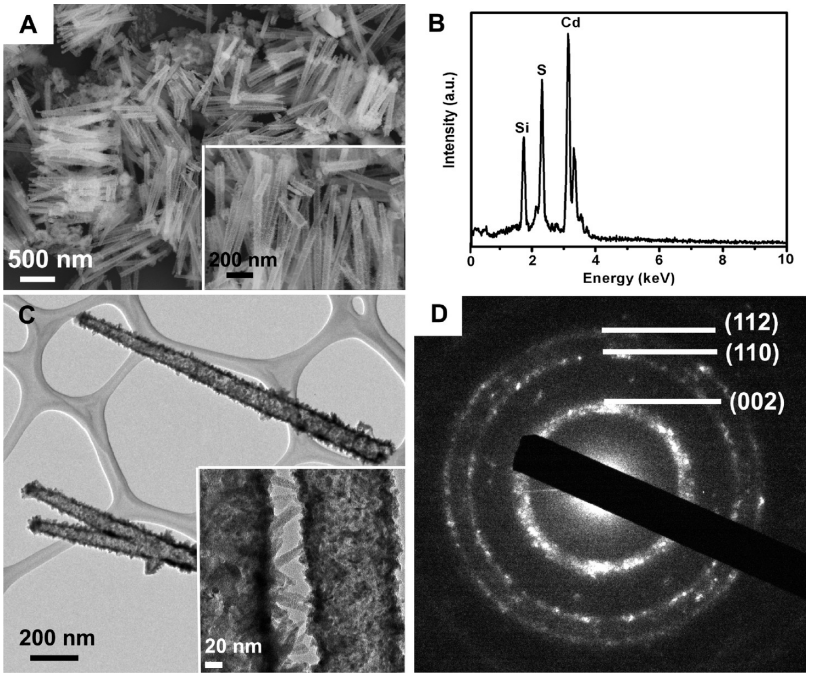

Figure 6. (A, C) Typical SEM and TEM images of as-prepared CdS cactus-like nanostructures, prepared using polycarbonate membranes with 100-nm pore diameters at 80 °C. Associated insets show a correspondingly magnified view of as-generated products. (B) EDS spectrum of as-prepared CdS cactus-like nanostructures. The Si peak originates from the underlying silicon wafer used for data collection. (D) SAED pattern of a representative portion of an individual CdS cactus-like nanostructure shown in (C).

highlighted in Figure 6C. The three rings observed can be indexed to the (002), (110), and (112) diffraction planes, respectively, corresponding to the crystalline hexagonal phase of CdS.

Figure 7A highlights a portion of a typical cactus-like nanostructure (e.g., inset to Figure 6C), constructed from needle-like bristles projecting outward and branching off from the main CdS nanotube framework. In this magnified view, it is evident that the outer wall of the tubes is almost completely covered with these thin nanoscale needles.

Representative HRTEM images were taken from three different positions along the length of the hierarchical nanostructure shown in Figure 7A. Namely, these included the bristle-coated inner wall of the nanotube (Figure 7B), the intersection region between the central "trunk" and the secondary bristles (Figure 7C), and finally, the constituent needle-like bristles themselves in a different area of the sample (Figure 7D), respectively. While it is difficult to conclusively demonstrate that we were able to directly probe the nanotube wall motif itself by means of HRTEM, the diffuse nature of the SAED pattern suggests that the entire "trunk" may have been polycrystalline in nature, and therefore, it is plausible to hypothesize that the "trunk" may have consisted of a multitude of multioriented single-crystalline domains. Indeed, a lattice spacing of ~0.339 nm, obtained from one of these nanocrystals (Figure 7B), can be ascribed to the (002) plane of a hexagonal würtzite CdS structure. Some of these nanocrystals may therefore have served as seeds for the adjoining branching structures.[70] We also observed the presence of defects such as stacking faults within the confluence areas between the central "trunk"

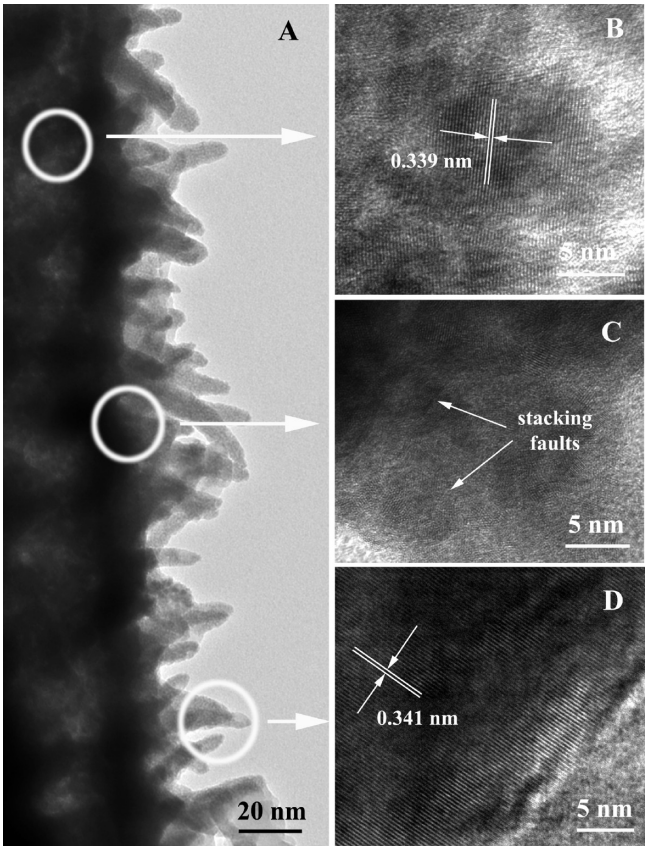

Figure 7. (A) TEM image of an individual CdS cactus-like nanostructure. (B−D) HRTEM images taken from various positions, delineated by white circles, respectively, along a portion of the cactus-like nanostructure in (A).

(70) Dick, K. A.; Deppert, K.; Larson, M. W.; Martensson, T.; Seifert, W.; Wallenberg, L. R.; Samuelson, L. *Nat. Mater.* **2004**, *3*, 380–384.

and its bristly "offshoots" (Figure 7C), similar to what has been previously described in analogous hierarchical systems.[71] Specifically, these stacking faults have been ascribed to the small energy difference between stacking sequences in the growth direction.[72] The bristles themselves maintain an obvious lattice spacing of ~0.341 nm, corresponding to the (002) planes of hexagonal CdS, an experimental result suggestive of the preferential [002] growth direction of these branched needle-like structures.

We have previously described, in detail, the formation of wires versus tubes using our modified template methodology.[48] In our specific experiments herein, it is generally believed that, at room temperature, single crystals of cubic CdS nanorods were derived from isolated, disparate nucleation sites, which then grew by extension throughout the porous network until contact was made with the confining membrane surface itself, acting as the ultimate barrier to growth. The hexagonal phase cactus-like nanostructure formation at 80 °C in the absence of surfactant is still a matter of study, but in the context of previous, analogous experiments by a multitude of groups, it can be explained as follows.

To account for the central nanotube "trunk", in prior work on α-Fe_2O_3, we have attributed tube-like formation to the fusion and coalescence of individual precursor particles preferentially localized along the surfaces of the template pore walls.[48] The observed formation of bristles or, alternatively, fractal dendritic structures in comparable systems has been previously ascribed to the nonequilibrium growth and the inherent molecular anisotropy of the hexagonal structure of CdS.[73,74] Diffusion-limited aggregation and nucleation-limited aggregation models have also been proposed to account for the formation of related complex hyperbranched structures.[72,75−78] Hence, in an alternate but plausible mechanism, with increasing temperatures, multiple nuclei, pertaining to the thermodynamically stable hexagonal phase of CdS, can form in solution in an initial nucleation stage. In the next step, these will subsequently grow to produce thin, well-crystallized CdS nanorods in the presence of additional "monomers", which randomly move about and subsequently accumulate with each other to create kinetically roughened fractal structures.[70,79−81] The lack of any definite, preferential angles with which the different branches emerged from the central trunk supports this "fractal" hypothesis in our system[79] since there were no additives present to "direct" growth. Furthermore, the diffusion of smaller CdS nanostructures is known to be faster at higher temperatures, which is also conducive to their aggregation.[82]

Raman Spectroscopy. The optical properties of these sulfide 1D nanostructures were also investigated. It is well known that in a crystalline semiconductor, the observed Raman shifts are usually associated with the longitudinal optical phonons (LO), while in general, other modes, such as the transverse optical phonons (TO) and the surface phonons (SP), are not as observable because of symmetry restrictions and weaknesses in the observed intensities, respectively.[83−85] However, these other modes can become viable due to surface roughness and crystallite size considerations as well as the large surface-to-volume ratio intrinsic to nanostructured materials. Therefore, Raman scattering measurements have become a unique tool for probing nanoscale vibrational properties, especially the exciton−phonon coupling through the Fröhlich interaction of multiexcitonic materials such as PbSe.[86]

Figure 8 highlights the Raman spectra of as-prepared semiconducting nanowires, corroborating the chemical identity of our as-prepared nanostructures. Specifically,a strong, sharp peak appearing at 470 cm^{-1} is dominant in the spectrum of CuS nanowires (Figure 8A) and has been previously associated with the covellite (CuS) system,[87−89] though we cannot necessarily preclude potential contributions from S−S stretching vibrational modes as well.[90]

Figure 8B displays the Raman spectrum of PbS nanowires. PbS is an inherently weak Raman emitter, but increasing the intensity of the laser excitation might have led to sample photo-oxidation.[86] One strong peak at 143 cm^{-1} is clearly observed, which can be ascribed to the SP mode.[91,92] According to earlier reports,[92,93] the intensity of this peak greatly increases with decreasing crystal size. We have found that this peak is so intense, though, that signals at 210 and 271 cm^{-1} resemble two small, secondary shoulders, corresponding to a 1 LO phonon mode and two-phonon mode process, respectively.[85,91] Our observation also suggests that the nanowire may be composed of a substructure of small

(71) Manna, L.; Scher, E. C.; Alivisatos, A. P. *J. Am. Chem. Soc.* **2000**, *122*, 12700–12706.
(72) Yao, W.-T.; Yu, S.-H.; Liu, S.-J.; Chen, J.-P.; Liu, X.-M.; Li, F.-Q. *J. Phys. Chem. B* **2006**, *110*, 11704–11710.
(73) Qingqing, W.; Gang, X.; Gaorong, H. *Cryst. Growth Des.* **2006**, *6* (8), 1776–1780.
(74) Ben-Jacob, E.; Godbey, R.; Goldenfeld, N. D.; Koplik, J.; Levine, H.; Mueller, T.; Sander, L. M. *Phys. Rev. Lett.* **1985**, *55*(12), 1315–1318.
(75) Halsey, T. C.; Duplantier, B.; Honda, K. *Phys. Rev. Lett.* **1997**, *78*, 1719–1722.
(76) Ming, N. B.; Wang, M.; Peng, R. W. *Phys. Rev. E* **1993**, *48*, 621–624.
(77) Witten, T.; Sander, L. M. *Phys. Rev. Lett.* **1981**, *47*, 1400–1403.
(78) Meakin, P. *Phys. Rev. A* **1983**, *27*, 1495–1507.
(79) Peng, Q.; Dong, Y.; Deng, Z.; Li, Y. *Inorg. Chem.* **2002**, *41*, 5249–5254.
(80) Qin, A.-M.; Fang, Y.-P.; Zhao, W.-X.; Liu, H.-Q.; Su, C.-Y. *J. Cryst. Growth* **2005**, *283*, 230–241.
(81) Hou, H.; Yang, Q.; Tan, C.; Tian, X.; Xie, Y. *Mater. Lett.* **2005**, *59*, 3364–3369.
(82) Zhao, P.; Huang, K. *Cryst. Growth Des.* **2008**, *8*(2), 717–722.
(83) Mlayah, A.; Brugman, A. M.; Carles, R.; Renucci, J. B.; Valakh, M. Y.; Pogorelov, A. V. *Solid State Commun.* **1994**, *90*, 567–570.
(84) Nanda, K. K.; Sahu, S. N. *Appl. Surf. Sci.* **1997**, *119*, 50–54.
(85) Wang, N.; Cao, X.; Guo, L.; Yang, S.; Wu, Z. *ACS Nano* **2008**, *2*, 184–190.
(86) Bierman, M. J.; Lau, Y. K. A.; Jin, S. *Nano Lett.* **2007**, *7*, 2907–2912.
(87) Rudigier, E.; Barcones, B.; Luck, I.; Jawhari-Colin, T.; Pérez-Rodríguez, A.; Scheer, R. *J. Appl. Phys.* **2004**, *95*, 5153–5158.
(88) Chen, G.-Y.; Deng, B.; Cai, G.-B.; Dong, W.-F.; Zhang, W.-X.; Xu, A.-W. *Cryst. Growth Des.* **2008**, *8*, 2137–2143.
(89) Minceva-Sukarova, B.; Najdoski, M.; Grozdanov, I.; Chunnilall, C. J. *J. Mol. Struct.* **1997**, *410−411*, 267–270.
(90) Bastian, E. J.; Martin, R. B. *J. Phys. Chem.* **1973**, *77*(9), 1129–1133.
(91) Ge, J.-P.; Wang, J.; Zhang, H.-X.; Wang, X.; Peng, Q.; Li, Y.-D. *Chem.—Eur. J.* **2005**, *11*, 1889–1894.
(92) Nanda, K. K.; Sahu, S. N.; Soni, R. K.; Tripathy, S. *Phys. Rev. B* **1998**, *58*, 15405–15407.
(93) Krauss, T. D.; Wise, F. W. *Phys. Rev. B* **1997**, *55*, 9860–9865.

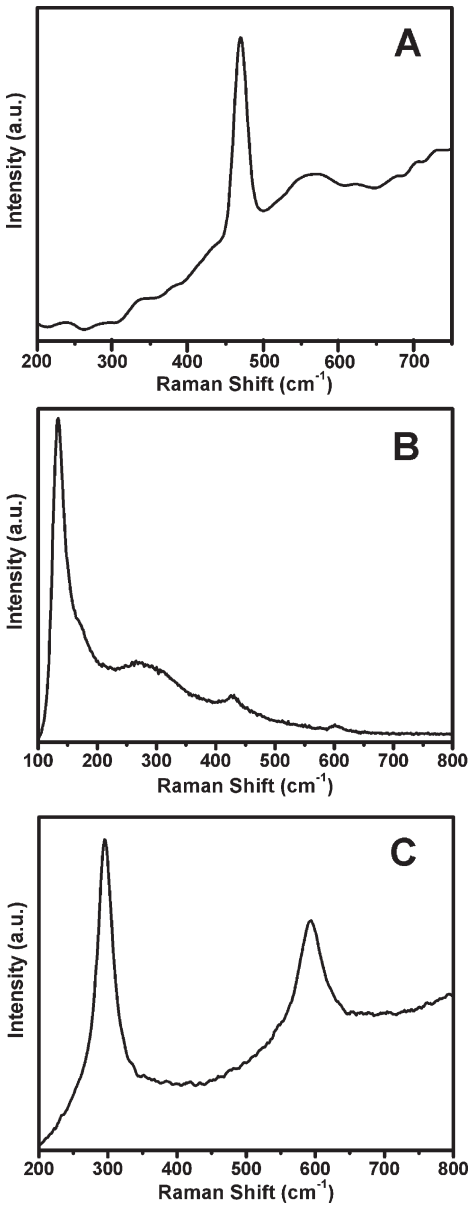

Figure 8. Raman spectra of as-prepared (A) CuS nanowires; (B) PbS nanowires; and (C) CdS nanowires.

discrete nanocrystals. The weak intensity of these peaks has been previously assigned to decreasing crystallite size,[92] which is also consistent with conclusions derived from our electron diffraction data. The Raman peak at 440 cm^{-1} can be assigned to a 2 LO phonon mode, that is, a broad overtone whose intensity is strongly dependent on the excitation wavelength.[93] Finally, the peak at 602 cm^{-1} has been previously ascribed to a second overtone signal.[85]

Figure 8C shows the Raman spectrum of as-prepared CdS nanowires. Two features of CdS are clearly evident, illustrating characteristic Raman shifts analogous to those of pure crystalline CdS.[38] Specifically, the two peaks located at 301 and 602 cm^{-1} can be assigned to the first- and second-order TO phonon modes, respectively,[58] though a number of groups have claimed that these peaks actually correspond to the fundamental LO band and its associated overtone.[37,84,94,95] Nonetheless, the observed phonon peaks are shifted toward lower frequency than would be expected from bulk, likely due to effects of small size and high surface area. Moreover, the relatively sharp and symmetric profile[56] of the peaks of our sample suggests that our nanorods are highly crystalline and relatively free of impurities, which concur with our electron microscopy data.

UV−Visible Spectroscopy. Figure 9 highlights the UV−visible absorption spectra of as-prepared transition metal sulfide nanowires, collected at room temperature. The absorption spectrum (Figure 9A) of CuS nanowires, which has been attributed by one group to partial oxidation of the nanowire surface,[96] showed a broad spectral band in the region between 300 and 650 nm. This result is in general agreement with prior reports,[88,97,98] with small peaks observed around 400 nm (i.e., 3.10 eV), potentially attributable to the nanorod morphology of the samples.[36] Previous studies[99] have shown that covellite CuS also possesses a characteristically broad absorption band beyond 800 nm, which extends as a long absorption tail into the near-IR region and that can be ascribed to an electron-acceptor state lying within the bandgap.[100−102] We have also observed data consistent with this interpretation.

The absorption spectrum of as-prepared PbS nanowires is shown in Figure 9B. It has been reported that isotropic spheres of PbS with a size less than 18 nm showed regular red-shifted excitonic absorption peaks from the visible to the infrared region with increasing particle size.[22,103] A red shift in absorption corresponding to 60 nm as compared with 30 nm PbS nanowires has also been observed.[104] We have detected a similar behavioral trend here with our relatively large-diameter nanorods. Nonetheless, the position of the absorption peak itself at 783 nm (i.e., 1.58 eV) is in agreement with a previous report.[105] By comparison, the expected PbS bulk absorption edge occurs at 3024 nm.[33,106] One plausible hypothesis for this observation, which was supported by the HRTEM/SAED data, is that the nanowires may consist of multiple single, crystalline domains composed

(94) Li, Y.; Liao, H.; Ding, Y.; Fan, Y.; Zhang, Y.; Qian, Y. *Inorg. Chem.* **1999**, *38*, 1382–1387.
(95) Kar, S.; Panda, S. K.; Satpati, B.; Satyam, P. V.; Chaudhuri, S. *J. Nanosci. Nanotechnol.* **2006**, *6*, 771–776.
(96) Wang, Q.; Li, J.-X.; Li, G.-D.; Cao, X.-J.; Wang, K.-J.; Chen, J.-S. *J. Cryst. Growth* **2007**, *299*, 386–392.
(97) Wang, W.; Ao, L. *Mater. Chem. Phys.* **2008**, *109*, 77–81.
(98) Jiang, X.; Xie, Y.; Lu, J.; He, W.; Zhu, L.; Qian, Y. *J. Mater. Chem.* **2000**, *10*, 2193–2196.
(99) Haram, S. K.; Mahadeshwar, A. R.; Dixit, S. G. *J. Phys. Chem.* **1996**, *100*, 5868–5873.
(100) Kalyanikutty, K. P.; Nikhila, M.; Maitra, U.; Rao, C. N. R. *Chem. Phys. Lett.* **2006**, *432*(1−3), 190–194.
(101) Xu, H.; Wang, W.; Zhu, W. *Mater. Lett.* **2006**, *60*, 2203–2206.
(102) Gao, J.; Li, Q.; Zhao, H.; Li, L.; Liu, C.; Gong, Q.; Qi, L. *Chem. Mater.* **2008**, *20*, 6263–6269.
(103) Watt, A.; Rubinsztein-Dunblop, H.; Mereidth, P. *Mater. Lett.* **2005**, *59*, 3033–3036.
(104) Wu, C.; Shi, J.-B.; Chen, C.-J.; Chen, Y.-C.; Wu, P.-F.; Lin, J.-Y. *Mater. Lett.* **2007**, *61*, 4659–4661.
(105) Ye, S.; Ye, Y.; Ni, Y.; Wu, Z. *J. Cryst. Growth* **2005**, *284*, 172–175.
(106) Wang, C.-W.; Liu, H.-G.; Bai, X.-T.; Xue, Q.; Chen, X.; Lee, Y.-I.; Hao, J.; Jiang, J. *Cryst. Growth Des.* **2008**, *8*, 2660–2664.

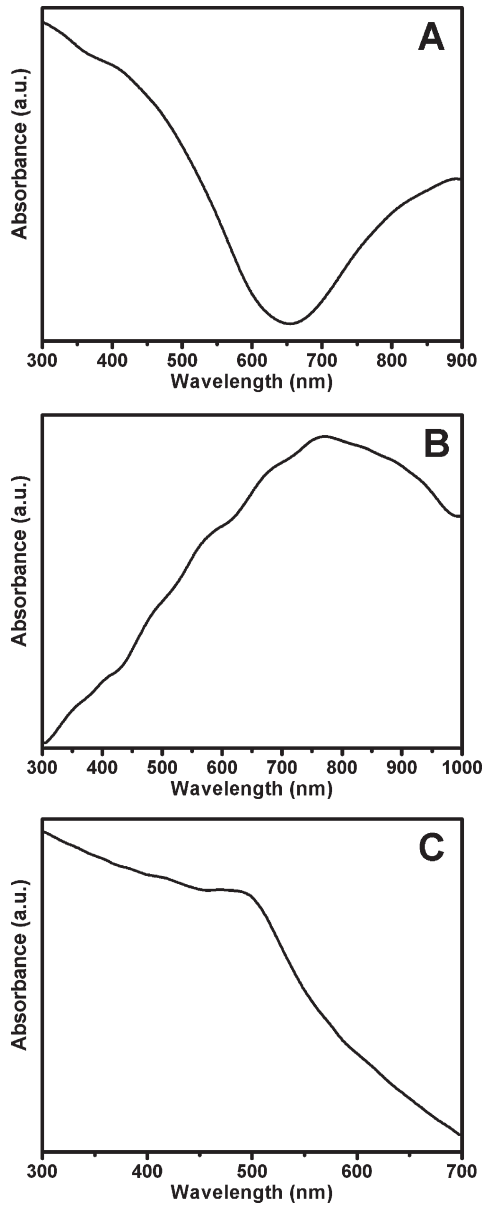

Figure 9. UV−visible spectra of as-prepared (A) CuS nanowires; (B) PbS nanowires; and (C) CdS nanowires.

of highly oriented nanocrystals smaller than the representative Bohr exciton radius of PbS.[107] Another reasonable explanation put forward for the presence of the excitonic absorption peak is that there are little if any surface defect sites on the nanorods that can trap electron−hole pairs generated by light.[106] By contrast, it was noted that PbS nanowires measuring 16 and 35 nm in diameter did not show any distinctive maximum in the infrared region of their absorption spectrum. The absence of such a sharp, band-edge absorption feature has also been attributed to convolution of absorption peaks from nanowires of different diameters as well as to the lack of confinement in the axial dimension of the wire.[108]

The UV−visible absorption spectrum of CdS nanowires is displayed in Figure 9C. The nanowires show a well-defined absorption feature at 498 nm (i.e., 2.49 eV), which can be ascribed to the first exciton peak of CdS.[109] This signal is considerably blue-shifted relative to the characteristic bulk band gap for hexagonal-phase CdS crystals (512 nm). In fact, the existence of a hexagonal CdS nanoscale impurity, the so-called minority phase, within the majority cubic phase was suggested by our XRD pattern (Figure 1C) and, thus, may have contributed to the observed UV absorption signal. These data are fully consistent with previous results.[72,82,109−116] It is worth noting that, as the cubic phase of CdS is not known in bulk form,[117] a direct band gap comparison could not be made.

While the origin of the observed blue shift, if real as it is convoluted with the broadness of the measured spectra, in all of these sulfide systems is debatable, one general explanation that has been put forward is that, in semiconductors, even if the average radius of the nanostructures were larger than that of the exciton Bohr radius, the Coulombic energy component is dominant.[36] Hence, motion (e.g., translational degrees of freedom) of the exciton, which behaves as a quasiparticle, experiences size quantization, thereby accounting for the shift to the blue.[118]

Photoluminescence Spectroscopy. The photoluminescent activity of all of our as-prepared transition metal sulfide nanowires was also probed, as shown in Figure 10. In particular, Figure 10A illustrates the room-temperature PL spectrum of the CuS nanowire sample dispersed in water. Under an excitation wavelength of 370 nm, the sample evinced an emission peak at 423 nm. Although the exact mechanism for explaining the nature of PL emission for CuS nanostructures remains controversial, prior literature suggests that the nature of the emission spectrum depends on the morphology and inherent microstructure of the sample itself. For instance, CuS needle-like fibers did not appear to evince any PL signal[98] in the range of 400−800 nm. However, polycrystalline CuS nanorods have been found to possess two emission peaks at 414 and 437.5 nm, upon excitation at 371.5 nm,[119] while as-prepared CuS/C cables yielded a broad but weak emission peak at 465 nm upon excitation at 370 nm.[88] Moreover, hollow spheres composed of polycrystalline nm-sized CuS crystals were associated with a broad emission with

(107) Wise, F. W. *Acc. Chem. Res.* **2000**, *33*, 773–780.
(108) Yong, K.-T.; Sahoo, Y.; Choudhury, K. R.; Swihart, M. T.; Minter, J. R.; Prasad, P. N. *Chem. Mater.* **2006**, *18*, 5965–5972.
(109) Xiong, Y.; Xie, Y.; Yang, J.; Zhang, R.; Wu, C.; Du, G. *J. Mater. Chem.* **2002**, *12*, 3712–3716.
(110) Wang, H.; Fang, P.; Chen, Z.; Wang, S. *J. Alloys Compd.* **2008**, *461*, 418–422.
(111) Yong, K.-T.; Sahoo, Y.; Swihart, M. T.; Prasad, P. N. *J. Phys. Chem. C* **2007**, *111*, 2447–2458.
(112) Nair, P. S.; Scholes, G. D. *J. Mater. Chem.* **2006**, *16*, 467–473.
(113) Liu, W.; He, W.; Zhang, Z.; Zheng, C.; Li, J.; Jiang, H.; Ge, X.; Liu, H. *J. Cryst. Growth* **2006**, *290*, 592–596.
(114) Maleki, M.; Mirdamadi, S.; Ghasemzadeh, R.; Sasani Ghamsari, M. *Mater. Lett.* **2008**, *62*, 1993–1995.
(115) Spahnel, L.; Anderson, M. *J. Am. Chem. Soc.* **1990**, *112*, 2278–2284.
(116) Ma, X.; Xu, F.; Liu, Y.; Liu, X.; Zhang, Z.; Qian, Y. *Mater. Res. Bull.* **2005**, *40*(12), 2180–2188.
(117) Banerjee, R.; Jayakrishnan, R.; Ayyub, P. *J. Phys., Condens. Mater.* **2000**, *12*, 10647–10654.
(118) Yoffe, A. D. *Adv. Phys.* **2002**, *51*(2), 799–890.
(119) Ou, S.; Xie, Q.; Ma, D.; Liang, J.; Hu, X.; Yu, W.; Qian, Y. *Mater. Chem. Phys.* **2005**, *94*, 460–466.

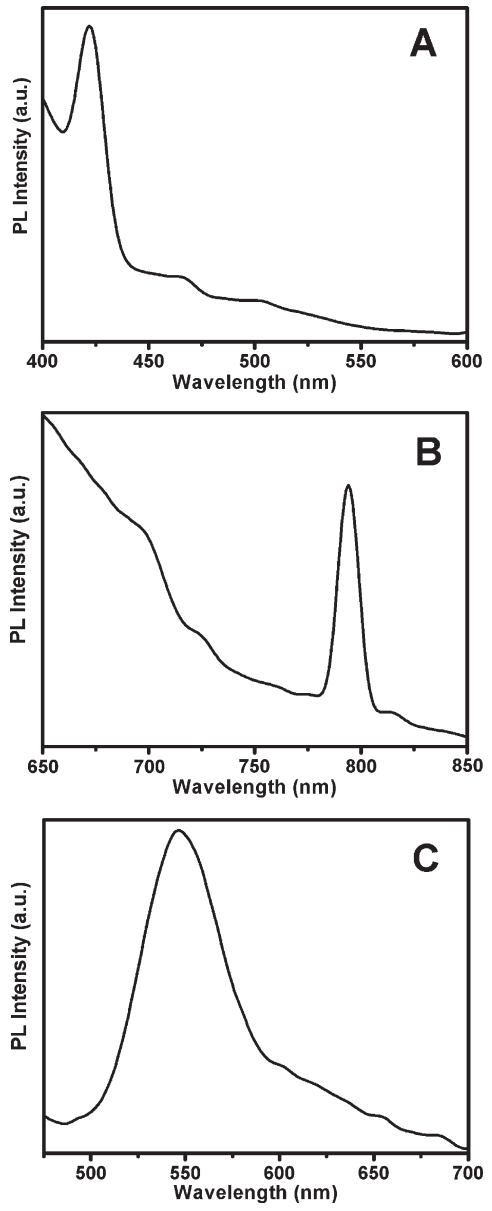

Figure 10. Photoluminescence spectra of as-prepared (A) CuS nanowires; (B) PbS nanowires; and (C) CdS nanowires, measured at room temperature.

a maximum at 526 nm upon excitation at 406 nm.[120] That result was explained by the presence of surface defects and an interface coupling effect between grain boundaries, thereby leading to an increase in wave function overlap and contributing to a narrower observable bandgap. Nonetheless, the sharp excitonic emission in our own results herein indicates that our as-prepared CuS nanowires are likely of high optical quality, since nanorods with stacking fault defects have been found to exhibit poor photoluminescence.[121]

The room-temperature PL spectrum of as-obtained PbS nanowires with an excitation wavelength of 495 nm is shown in Figure 10B. The fluorescence of PbS nanostructures is generally rather weak in intensity but detectable in the visible region.[122] A rather sharp PL band has been clearly observed at 794 nm (i.e., red fluorescence) (Figure 9B) and is blue-shifted as compared with bulk.[105,123] Others have reported a PL peak for nanoscale PbS in the 655−665 nm range, which has been ascribed to a transition associated with the lowest energy exciton.[35,44,124] Our results are in agreement with and understandably red-shifted with respect to data obtained on < 10 nm PbS nanoparticles, wherein the strong emission response was assigned to band edge luminescence (BEL).[22,125,126] Again, our observations are consistent with the idea that our as-prepared nanowires may be plausibly composed of multiple single domains of PbS quantum dots.

Figure 10C denotes the PL spectrum of as-prepared CdS nanowires, obtained with an excitation wavelength of 400 nm at room temperature. Though the intensity of the peak has been previously attributed to the presence of surface defects,[42] a relatively sharp emission peak at 547 nm was detected, analogous to previously reported results.[42,60,127] This band has been ascribed to near-band-edge (NBE) emission, originating from the recombination of excitons and/or shallowly trapped electron hole pairs within surface states.[56,59,95,113,127,128] We also note the relative narrowness of the PL peak, coupled with the lack of a strong emission near 600 nm from deep levels associated with defects (such as vacancies and interstitials)[82,129] and impurities.[12,130] In fact, the lack of a broad, longer-wavelength, trap emission state, which would have resulted from an excess of either sulfur or cadmium at the interface and which is known to quench radiative recombination of electron hole-pairs,[131] strongly suggests the high degree of purity of our samples. Overall, our results intimate that our single-crystalline nanowires have high-quality optical properties, critical for photonic device applications, and also possess a reasonable size monodispersity in terms of diameter and length.[57]

Photocatalytic Activity. In terms of photoinduced degradation reactions, it is known that under UV light irradiation, in the presence of CdS nanocrystals, halogenated benzenes are often dehalogenated, yielding trichlorobenzene from hexachlorobenzene and tetrafluorobenzene isomers from hexafluorobenzene as the final

(120) Yu, X.; Cao, C.; Zhu, H.; Li, Q.; Liu, C.; Gong, Q. *Adv. Funct. Mater.* **2007**, *17*, 1397–1401.
(121) Roy, P.; Mondal, K.; Srivastava, S. K. *Cryst. Growth Des.* **2008**, *8*, 1530–1534.
(122) Machol, J. L.; Wise, F. W.; Patel, R.; Tanner, D. B. *Phys. A* **1994**, *207*, 427–434.
(123) Acharya, S.; Gautam, U. K.; Sasaki, T.; Bando, Y.; Golan, Y.; Ariga, K. *J. Am. Chem. Soc.* **2008**, *130*, 4594–4595.
(124) Patla, I.; Acharya, S.; Zeiri, L.; Israelachvili, J.; Efrima, S.; Golan, Y. *Nano Lett.* **2007**, *7*, 1459–1462.
(125) Chen, S.; Truax, L. A.; Sommers, J. M. *Chem. Mater.* **2000**, *12*, 3864–3870.
(126) Kim, D.; Kuwabara, T.; Nakayama, M. *J. Lumin.* **2006**, *119−120*, 214–218.
(127) Wang, W.; Germanenko, I.; El-Shall, M. S. *Chem. Mater.* **2002**, *14*, 3028–3033.
(128) Kar, S.; Chaudhuri, S. *J. Phys. Chem. B* **2006**, *110*, 4542–4547.
(129) Mondal, S. P.; Dhar, A.; Ray, S. K. *Mater. Sci. Semicond. Proc.* **2007**, *10*, 185–193.
(130) Pike, R. D.; Cui, H.; Kershaw, R.; Dwight, K.; Wold, A.; Blanton, T. N.; Wernberg, A. A.; Gysling, H. J. *Thin Solid Films* **1993**, *224*, 221–226.
(131) Hsu, Y.-J.; Lu, S.-Y. *Langmuir* **2004**, *20*, 23–26.

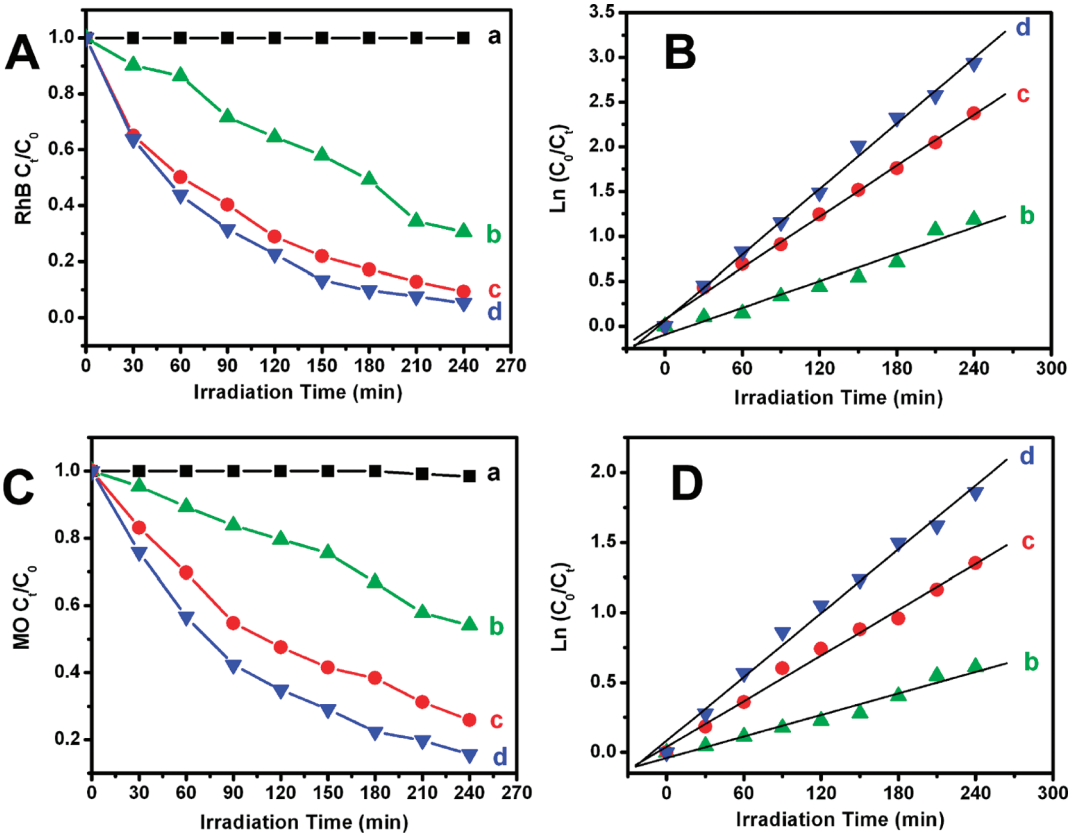

Figure 11. (A) Photodegradation of Rhodamine B (RhB) in the presence of (a, black) a blank control, (b, green) a commercial CdS bulk sample, (c, red) as-prepared CdS nanowires, and (d, blue) as-prepared CdS cactus nanostructures. (B) Plot of the logarithmic change in concentration of RhB as a function of irradiation in the presence of (b, green) a commercial CdS bulk sample, (c, red) as-prepared CdS nanowires, and (d, blue) as-prepared CdS cactus nanostructures. (C) Photodegradation of methyl orange (MO) in the presence of (a, black) a blank control, (b, green) a commercial CdS bulk sample, (c, red) as-prepared CdS nanowires, and (d, blue) as-prepared CdS cactus nanostructures. (D) Plot of the logarithmic change in concentration of MO as a function of irradiation in the presence of (b, green) a commercial CdS bulk sample, (c, red) as-prepared CdS nanowires, and (d, blue) as-prepared CdS cactus nanostructures.

products.[132] It is obvious though that the analogous roles of crystal phase, grain size, phase composition, and dimensionality have not been determined for photodegradation reactions of nonbiodegradable organic dyes, which are model organic substrates, representative of organic pollutant systems.

Thus, in this work, we probed reasonably simple reactions involving the degradation of Rhodamine B and methyl orange under UV irradiation conditions in the presence of CdS.[133,134] The photocatalytic potential of as-prepared CdS nanowires was evaluated by monitoring the optical behavior of Rhodamine B (RhB) and methyl orange (MO) at their peak absorbances upon photoexcitation with UV light at 366 nm. We noted a continual fading of the coloration of both RhB and MO solutions as a function of reaction time, in the presence of CdS nanowires, cactus-like nanostructures, or commercial bulk samples, implying a steady, continuous degradation of the organic dyes.

As shown in Figure 11A, the photocatalytic performance of CdS was estimated by monitoring the intensity of RhB's characteristic absorption at 555 nm as a function of reaction time. The data clearly showed that nanowires, cactus-like nanostructures, and the bulk sample are active photocatalysts, as illustrated in Figure 11A,b−d. In addition, both CdS nanowires and cactus-like nanostructures exhibited a higher photocatalytic degradation activity as compared with the bulk sample. The photocatalytic activity of CdS was also evaluated by probing the analogous degradation of MO molecules in water, by measuring changes in absorption at 464 nm (Figure 11C, b−d) as a function of reaction time. Similar trends were observed in that the CdS nanowires and cactus-like nanostructures yielded an appreciably higher activity as compared with bulk behavior. As control experiments, we observed almost no dye degradation in solution, in the absence of CdS catalyst, similarly subjected to UV light irradiation.

The photocatalytic decolorization reaction of RhB can be modeled as a pseudo-first-order reaction with the kinetics expressed by the equation, $\ln(C_0/C_t) = kt$, where C_0 represents the initial concentration of aqueous RhB, C_t denotes the concentration of RhB at a given reaction time "t", and k is the reaction rate constant. From the linear extrapolations (Figure 11B), the computed reaction rate constants of the CdS cactus-like nanostructures, nanowires, and bulk sample are 1.2×10^{-2} min^{-1},

(132) Yin, H.; Wada, Y.; Kitamura, T.; Yanagida, S. *Environ. Sci. Technol.* **2001**, *35*, 227–231.
(133) Li, W.; Li, D.; Chen, Z.; Huang, H.; Sun, M.; He, Y.; Fu, X. *J. Phys. Chem. C* **2008**, *112*, 14943–14947.
(134) Guo, Y.; Zhang, H.; Wang, Y.; Liao, Z.-L.; Li, G.-D.; Chen, J.-S. *J. Phys. Chem. B* **2005**, *109*, 21602–21607.

9.5×10^{-3} min^{-1}, and 4.9×10^{-3} min^{-1}, respectively. For the corresponding degradation rates of MO in the presence of these various CdS morphologies, Figure 11D demonstrates calculated first-order reaction rate constants of 7.6×10^{-3} min^{-1}, 5.5×10^{-3} min^{-1}, and 2.6×10^{-3} min^{-1} for CdS cactus-like nanostructures, nanowires, and bulk samples, respectively.

The potential photocatalytic mechanism in the degradation of RhB and MO has been previously described and may involve several steps: (1) photoabsorption of the CdS catalysts, (2) generation of photoinduced electrons and holes, (3) transfer of charge carriers to the surface, and (4) recombination of the available charge carriers with reactive, reagent dye molecules.[133] The observed enhancement of photocatalytic activity of our as-prepared nanowires and cactus-like nanostructures herein is most likely correlated with an increase in the purity, crystallinity, and availability of surface reactive sites of our samples as compared with the bulk. This structural morphology-dependent trend is also consistent with our previous results on analogous semiconducting nanoparticle systems.[46,48] Moreover, in the case of cactus-like nanostructures, the hexagonal phase CdS is generally considered to be the more efficient phase for photocatalysis-related applications.[135,136]

A previous report on the photocatalytic degradation of RhB, under identical UV light irradiation conditions in the presence of cubic CdS nanocrystals measuring ~3 nm implanted in a metal hydroxide layer matrix, showed that the amount of observed dye decomposition was up to 95% after 100 min of UV light irradiation.[134] By contrast, our unbound samples necessitated about 135 min to achieve an identical degree of dye degradation. The superior photocatalytic performance of those nanocrystals was attributed to the more effective migration of photoinduced holes and electrons to the nanoparticle surface and their associated trapping at the interface between the nanoparticle and its solid layer matrix.

(135) Matsumura, M.; Furukawa, S.; Saho, Y.; Tsubomura, H. *J. Phys. Chem.* **1985**, *89*, 1327–1329.
(136) Silva, L. A.; Ryu, S. Y.; Choi, J.; Choi, W.; Hoffmann, M. R. *J. Phys. Chem. C* **2008**, *112*, 12069–12073.

Conclusions

The current report demonstrates the reliable, reproducible, room-temperature synthesis, using a modified template-directed methodology, of crystalline semiconducting metal sulfide (CuS, PbS, and CdS) nanowires, with various controllable sizes and shapes including vertically aligned arrays and temperature-dependent cactus-like assemblies. The porous channels of our polycarbonate membranes not only enable the continuous flow of precursor solution but also provide for a spatially constrained environment to direct the growth of sulfide nanowires. Structural imperfections in our samples, such as protrusions and depressions, directly reflected the interior nanoscopic profiles of the template pore channels from whence these nanomaterials were derived. Our resulting 1D nanostructures have been extensively characterized using a variety of diffraction, electron microscopy, and optical spectroscopy techniques. Moreover, for the first time, we have demonstrated that as-prepared CdS nanowires, ambiently generated and possessing a pure cubic phase, show potential applications in the photocatalytic degradation of organic dyes.

Acknowledgment. We acknowledge the U.S. Department of Energy (DE-AC02-98CH10886) for generous facility and personnel support. We also thank the National Science Foundation (CAREER Award DMR-0348239) and the Alfred P. Sloan Foundation for PI support and experimental supplies. Moreover, we are grateful to Dr. Dezhi Wang at Boston College, as well as Dr. James Quinn and Dr. Susan van Horn at SUNY Stony Brook for their invaluable help with electron microscopy. We appreciate the assistance of Dr. Mandakini Kanungo with Raman analyses.

Supporting Information Available: Literature review on prior nanoscale metal sulfide studies, comments on photocatalytic activity, crystallographic data, SEM images, and XRD patterns (PDF). This material is available free of charge via the Internet at http://pubs.acs.org.